Technical Notes

Three-Dimensional Laser–Fluid Interaction Solver Within the OpenFOAM Framework

Vikramank Singh,* Kowsik Bodi,† and Aniruddha Sinha‡
Indian Institute of Technology Bombay, Mumbai 400 076, India

https://doi.org/10.2514/1.T7232

Downloaded by Indian Institute of Technology, Bombay on November 26, 2025 | http://arc.aiaa.org | DOI: 10.2514/1.T7232

I. Introduction

HIGH-ENERGY lasers have a wide range of industrial applications, including cutting, welding, machining, and directed energy systems [1,2]. They also hold promise in diverse fields such as laser beam propulsion, rock drilling, and wireless power transfer [1,3,4]. After generation, the laser beam propagates inside the beam director and then travels through the atmosphere before reaching the target. When a high-energy laser beam propagates through a fluid medium, the fluid medium gets heated due to the absorption of the laser beam photons by the molecules of the medium. This heating changes the fluid's temperature, and thus its density and refractive index. The changed refractive index of the fluid medium then distorts the laser beam passing through it, which again affects the fluid's refractive index. Thus, the laser beam intensity distribution in the three-dimensional space and the refractive index of the medium affect each other in a coupled manner. The presence of natural convection due to gravity further complicates this laser–fluid interaction, leading to beam deterioration. Initially, when the convection effects are insignificant, the refractive index decreases due to the expansion of the fluid in the laser's path, forming a negative lens. This results in the swelling of the beam profile, a phenomenon known as thermal blooming. Thermal blooming is a well-reported phenomenon [5].

In the atmosphere, when a laser beam is slewed for targeting or when wind is present transverse to the beam axis, the laser beam experiences a normal flow that sweeps away the heated air. Conventionally, laser–fluid interaction has been studied in the presence of a prescribed transverse flow [6–9]. Fleck, Morris, and Feit conducted a detailed study on laser beam propagation in the presence of horizontal wind at subsonic, transonic, and supersonic speeds [9]. The presence of external flow or wind modifies the fluid dynamics of the medium because the thermal convection effect induced by the applied flow dominates other effects. However, this also simplifies the computations. The effect of atmospheric turbulence on the laser beam has been simulated using discrete random phase screens, and adaptive optics have been employed to mitigate beam distortions [8,10]. To include the effect of buoyancy, Akers and Reeger solved the fluid dynamics in two-dimensional planes transverse to the beam motion, and interpolated the results to obtain the three-dimensional temperature field [11]. This method is limited to cases where convection is normal to the beam propagation direction and temperature gradients along the propagation direction are negligible.

Within the laser beam delivery system, after beam generation, the laser beam passes through various optical components that adjust its size and direction, before it exits through the beam director's window [12,13]. While traveling between mirrors and lenses inside the beam director, the laser beam interacts with the surrounding fluid and becomes distorted. Understanding these laser-induced distortions within the beam delivery system is essential for the development of more efficient and powerful high-energy laser devices.

To investigate laser–fluid interactions within closed domains accounting three-dimensional fluid dynamics, we have developed and validated a solver, `icoLfiFoam`, in the OpenFOAM environment. The novelty of the work lies in the implementation of the laser propagation solver coupled with a conventional finite volume flow solver, as well as its application to laser–fluid interaction in confined spaces.

In studies involving laser heating phenomena, predefined heat profiles are typically assumed [14,15]. In aero-optics problems, only one-way interactions are considered, where the optical beam is distorted by the turbulent flowfield over the optical surface [16–18]. For directed energy applications at the surface of flying targets, the physics is governed by coupled beam–flow interactions [14,18]. In our solver, the laser and fluid are simulated in a fully coupled manner, allowing the heating profile to evolve dynamically in both space and time due to laser distortions. This approach can be further extended using a compressible flow solver to study laser–target interactions.

II. Mathematical Formulation

Our objective is to simulate the interaction between the laser beam and the fluid medium as it propagates between two optical systems within a beam director. We model a section of the beam director, between these two optical systems, as a closed domain. In this domain, the laser enters at one end, passes through the fluid medium, and exits at the opposite end. The laser beam properties at the exit are the primary metrics of interest. In the computational domain, the fluid adheres to physical boundary conditions while the laser remains sufficiently distant from the sidewalls along the beam propagation direction.

Given practical conditions and laser power, the temperature increase caused by the absorption of a continuous laser beam propagating through the fluid is minimal. Fluid dynamics is thus governed by the incompressible Navier–Stokes equations under the Boussinesq approximation [19]:

$$\nabla \cdot \boldsymbol{u} = 0 \tag{1a}$$

$$\frac{\partial \boldsymbol{u}}{\partial t} + \nabla \cdot (\boldsymbol{u}\boldsymbol{u}) = \nu \nabla^2 \boldsymbol{u} - \frac{1}{\rho_0}\nabla p + \frac{T - T_0}{T_0}\boldsymbol{g} \tag{1b}$$

$$\frac{\partial T}{\partial t} + \nabla \cdot (T\boldsymbol{u}) = \alpha \nabla^2 T + s \tag{1c}$$

Here, $\boldsymbol{u}$ represents velocity vector; p represents pressure; T represents temperature; ν is the kinematic viscosity; α is the thermal

Presented as Paper 2025-2494 at the AIAA SciTech Forum, Orlando, FL, January 6–10, 2025; received 14 March 2025; accepted for publication 7 August 2025; published online 9 September 2025. Copyright © 2025 by Vikramank Singh. Published by the American Institute of Aeronautics and Astronautics, Inc., with permission. All requests for copying and permission to reprint should be submitted to CCC at www.copyright.com; employ the eISSN 1533-6808 to initiate your request. See also AIAA Rights and Permissions https://aiaa.org/publications/publish-with-aiaa/rights-and-permissions/.

*Ph.D. Student, Department of Aerospace Engineering; vikramankpratapsingh@gmail.com (Corresponding Author).

†Associate Professor, Department of Aerospace Engineering. Member AIAA.

‡Associate Professor, Department of Aerospace Engineering. Member AIAA.

diffusivity; and T_0 and ρ_0, respectively, represent the initial temperature and density of the medium. In the energy equation, a source term s is added to account for the temperature increase resulting from laser absorption by the fluid medium. Additionally, $\boldsymbol{g}$ refers to the gravitational acceleration vector.

The local (complex) amplitude of the laser is denoted by A. The propagation of the laser beam through the fluid medium, under the paraxial approximation ($|\partial A/\partial z| \ll |kA|$), is described by the paraxial equation [20]:

$$2ik\frac{\partial A}{\partial z} = A_{xx} + A_{yy} + k^2\left(\frac{n^2}{n_0^2} - 1\right)A - ik(\beta_a + \beta_s)A \tag{2}$$

Here, z is the direction of beam propagation, while x and y are the orthogonal directions, and i is the square root of negative unity. Laser beam intensity and amplitude are related by $I = |A|^2$. The wave number of the beam is denoted by k, whereas $n(x, y, z; t)$ represents the refractive index of the medium, and n_0 represents the initial ($t = 0$) refractive index of the medium. Absorption and scattering coefficients of the medium are represented by β_a and β_s, respectively. The refractive index and temperature are related using the following relation (derived from a Taylor series expansion):

$$\frac{n^2}{n_0^2} - 1 = 2\frac{(T - T_0)}{n_0}\frac{dn}{dT} \tag{3}$$

Here, dn/dT is a property of the medium, representing the rate of change of refractive index with temperature. It is typically a negative value, meaning the refractive index decreases as the temperature increases.

The volumetric heat absorption rate by the fluid medium due to laser heating is $\beta_a I$. Hence, the corresponding rate of temperature change in the medium due to laser heating is given by $s = \beta_a I/\rho_0 c_p$, where c_p denotes the specific heat capacity of the fluid.

III. Solution Methodology

The solution of Eqs. (1) and (2) with the appropriate initial and boundary conditions yields results for laser–fluid interaction. We selected `icoFoam`, a validated transient incompressible laminar flow solver within the OpenFOAM library, for solving the fluid dynamics [21]. OpenFOAM is structured to handle any time-dependent partial differential equation (PDE) having convection, diffusion, and source terms [22]. The paraxial equation is a complex PDE, parabolic in the z-direction, and it does not have any time dependence (i.e., because the laser propagation timescale is minuscule relative to the flow timescale). We split the paraxial equation of variable $A = A_r + iA_i$ into two PDEs of real variables A_r and A_i. We solve two equivalent real equations instead of a single complex one. Equation (2) is a parabolic equation that is solved numerically by marching along the beam propagation direction, i.e., z. To the best of our knowledge, OpenFOAM does not have in-built modules that allow this space-marching approach. Hence, we explicitly added the computation of the paraxial equation within the `icoLfiFoam` solver using basic C++ syntax.

The fluid at the $(j + 1)$th time step is solved using the laser intensity field at the jth time step, and the laser amplitude is corrected at the $(j + 1)$th time step using the refractive index field at the same step. We used the split-step spectral method to solve the paraxial equation [23,24]. In this method, the paraxial equation is split into two parts:

$$2ik\frac{\partial A}{\partial z} = k^2\left(\frac{n^2}{n_0^2} - 1\right)A - ik(\beta_a + \beta_s)A \tag{4a}$$

$$2ik\frac{\partial A}{\partial z} = A_{xx} + A_{yy} \tag{4b}$$

First, Eq. (4a) is solved by integration over Δz, yielding

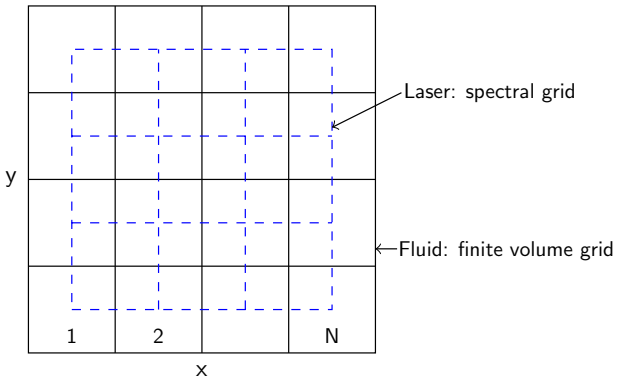

Fig. 1 Laser–fluid grid in the plane perpendicular to the beam propagation direction.

$$A^\star = A(x, y, z)\exp\left[\left(\frac{n^2}{n_0^2} - 1\right)\frac{k\Delta z}{2i} - \frac{(\beta_a + \beta_s)\Delta z}{2}\right] \tag{5}$$

This intermediate field $A^\star$ is then used as the initial condition to solve Eq. (4b). To compute the laser amplitude at the $z + \Delta z$ location, the $n^2/n_0^2 - 1$ value used is calculated using the average temperature between the z and $z + \Delta z$ planes. For improved accuracy over other numerical methods and ease of implementation, Eq. (4b) is solved using the spectral method. In the spectral domain, Eq. (4b) takes the form

$$2ik\frac{d}{dz}\mathcal{F}_{k_x,k_y}A = -(k_x^2 + k_y^2)\mathcal{F}_{k_x,k_y}A \tag{6}$$

where k_x and k_y represent the wave numbers in the x and y directions, respectively. The operator $\mathcal{F}_{k_x,k_y}$ denotes the forward Fourier transform. After integration over Δz, the solution in the spectral domain is

$$\mathcal{F}_{k_x,k_y}A = (\mathcal{F}_{k_x,k_y}A^\star)\exp\left[-\frac{(k_x^2 + k_y^2)\Delta z}{2ik}\right] \tag{7}$$

The spatial domain solution A for all x–y at $z + \Delta z$ is retrieved via the inverse Fourier transform:

$$A(x, y, z + \Delta z) = \mathcal{F}_{x,y}^{-1}\left(\mathcal{F}_{k_x,k_y}A\right) \tag{8}$$

where $\mathcal{F}_{x,y}^{-1}$ represents the inverse Fourier transform. Fourier operations are executed within the `icoLfiFoam` solver using the FFTW library [25]. The laser beam profile on the first x–y plane ($z = 0$) serves as the initial condition. The split-step method ensures numerical stability and efficiency.

While the spectral method is a node based method, OpenFOAM solves fluid variables at the cell centers using the finite volume method. For a uniform grid, the grid nodes for the paraxial equation variable coincide with the cell centers of the grid for the fluid variables in the x, y directions as represented in Fig. 1. The laser grid is periodic, with the laser amplitude solved at each z plane on $(N - 1) \times (N - 1)$ nodes. The laser domain is truncated by half a grid size at both ends in the x and y directions. Since the laser remains far from the sidewalls, the laser amplitude drops to zero near the walls, eliminating the need for additional boundary treatments. The laser amplitude at the Nth nodes is set equal to its value on the respective first nodes in the x and y directions.

IV. Solver Validation

A. Laser Propagation in Vacuum

When a laser beam propagates through a vacuum, diffraction causes the beam to diverge. At the source ($z = 0$), the intensity of a Gaussian beam is defined as

Downloaded by Indian Institute of Technology, Bombay on November 26, 2025 | http://arc.aiaa.org | DOI: 10.2514/1.T7232

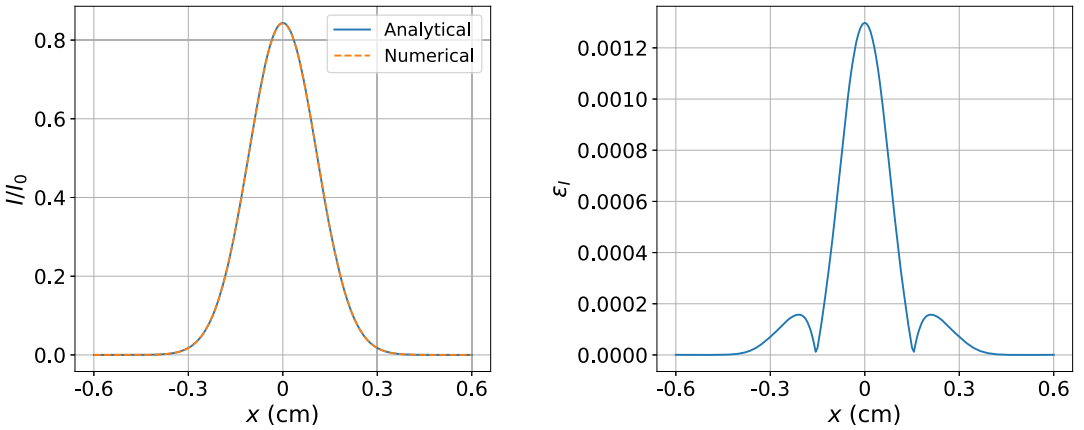

Fig. 2 Comparison of numerical and analytical solutions for laser beam propagation in a vacuum, with plots of I/I_0 and the error ($\epsilon_I = (|I_{\text{true}} - I|)/I_0$) at $y = 0$ and $z = 50$ cm as functions of x.

$$I(x, y, 0; t) = I_0 e^{-\frac{x^2+y^2}{r^2}} \tag{9}$$

Here, I_0 represents the peak laser intensity at the source and r represents the laser beam's initial radius (between 1 and 1/e intensity points). It is calculated using the laser power at source P_0 and the radius using the relation $I_0 = P_0/\pi r^2$.

For a continuous Gaussian beam of wavelength λ and radius r, propagating through a medium of constant refractive index n, laser beam intensity distribution after propagating through distance z is [26]

$$I(x, y, z) = I_0 \left(\frac{r}{r(z)}\right)^2 \exp\left(-\frac{x^2 + y^2}{r(z)^2}\right) \tag{10}$$

Here,

$$r(z) = r\sqrt{1 + \left(\frac{z\lambda}{2\pi r^2 n}\right)^2} \tag{11}$$

is the beam radius at distance z.

For a laser beam of power 11 W, wavelength of 10.6 μm, and radius of 1.4 mm, the intensity profile after propagating for 0.5 m through a vacuum ($n = 1$) was calculated using the `icoLfiFoam` solver. We used a computational domain of size $1.2 \times 1.2 \times 50$ cm^3 discretized into a $201 \times 201 \times 40$ grid. The laser beam was sourced at $x = 0, y = 0$ in the $z = 0$ plane. At the end of the domain ($z = 50$ cm), the numerical results were compared to the analytical solution I_{true}, showing good agreement, as illustrated in Fig. 2. Because the medium is vacuum, the values of all fluid dynamic variables are zero.

B. Moving Laser in Fluid

Another validation of the developed `icoLfiFoam` solver is conducted based on the laser thermal distortion experiment by Gebhardt and Smith [7]. In their experiment, a laser beam was directed through a high-absorptivity fluid in a cylindrical cell of 5 cm in diameter and 2.5 cm in length. The cell was made to move at a constant speed perpendicular to the laser beam propagation direction. The resulting laser distortion was reported. To replicate their experiment, for ease of computation, we have taken a cuboid-shape computational domain of dimensions $L_x \times L_y \times L_z$ as shown in Fig. 3, where L_x, L_y, and L_z are the domain lengths along the x, y, and z axes, respectively. The dimensions of the cuboid are taken as $L_x = L_y = 3.54$ cm (which is $1/\sqrt{2}$ times the diameter of the cylindrical cell used in the reference experiment) and $L_z = 2.5$ cm, inscribing the maximal cuboid within the cylindrical cell of the experiment.

In this setup, a continuous Gaussian laser beam with a wavelength of 10.6 μm and a radius of 1.4 mm is introduced from the $z = 0$ plane. The fluid medium is carbon disulfide (CS_2), with thermophysical and optical properties: $dn/dT = -0.79 \times 10^{-3}$ K^{-1}, $\alpha = 1.25 \times 10^{-7}$ m$^2 \cdot$ s^{-1}, $\nu = 2.86 \times 10^{-7}$ m$^2 \cdot$ s^{-1}, $\beta_a = 25.2$ m^{-1}, $c_p = 950$ J/kg$^{-1} \cdot$ K^{-1}, $n_0 = 1.63$, $\rho_0 = 1260$ kg/m^{-3}, and $T_0 = 300$ K. Consistent with the reference study by Gebhardt and Smith [7], scattering effects are neglected by setting $\beta_s = 0$. This fluid has an exceptionally high absorption coefficient, which leads to significant beam distortion over a short propagation path, even with a laser beam of modest power. The laser beam is moving with respect to the domain along the negative x direction. All the boundaries of the fluid domain are considered as free-slip isothermal walls. We considered free-slip walls because we are not interested in resolving the boundaries, especially along the z direction. Based on our numerical trials, free-slip isothermal walls provide better stability as compared to no-slip adiabatic walls. Moreover, the experimental domain is a cylindrical cell, whereas our computational domain is a cuboid rendering the boundary condition treatment moot.

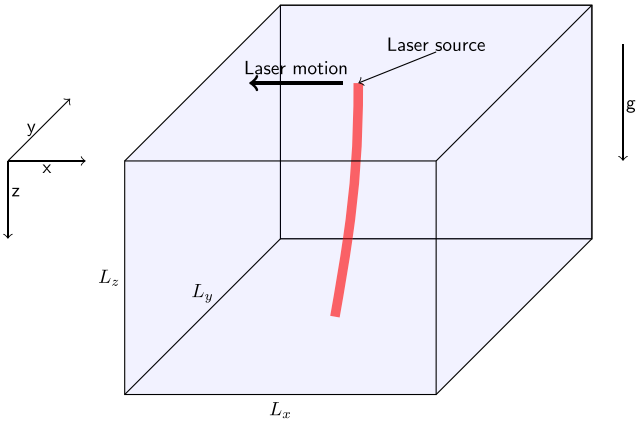

Fig. 3 Illustration of the computational domain for moving laser problem.

We performed numerical simulations for laser powers of 1, 5, and 11 W with a laser velocity relative to the fluid domain u of 0.9 cm/s. After conducting a grid independence test, we selected a $601 \times 601 \times 40$ uniform grid. The beam distortion parameter N_D, defined by Gebhardt and Smith, was calculated for each laser power using the following expression [7]:

$$N_D = \frac{-2(dn/dT)I_0 L_z}{n_0 \rho_0 c_p u r}\left(1 - \frac{1 - e^{-\beta_a L_z}}{\beta_a L_z}\right) \tag{12}$$

At the start of the simulation ($t = 0$ s), the laser beam source is positioned at the mid-xz plane ($y = L_y/2$) near the right wall. We compared the laser beam intensity profiles at $t = 1.8$ s from the

Downloaded by Indian Institute of Technology, Bombay on November 26, 2025 | http://arc.aiaa.org | DOI: 10.2514/1.T7232

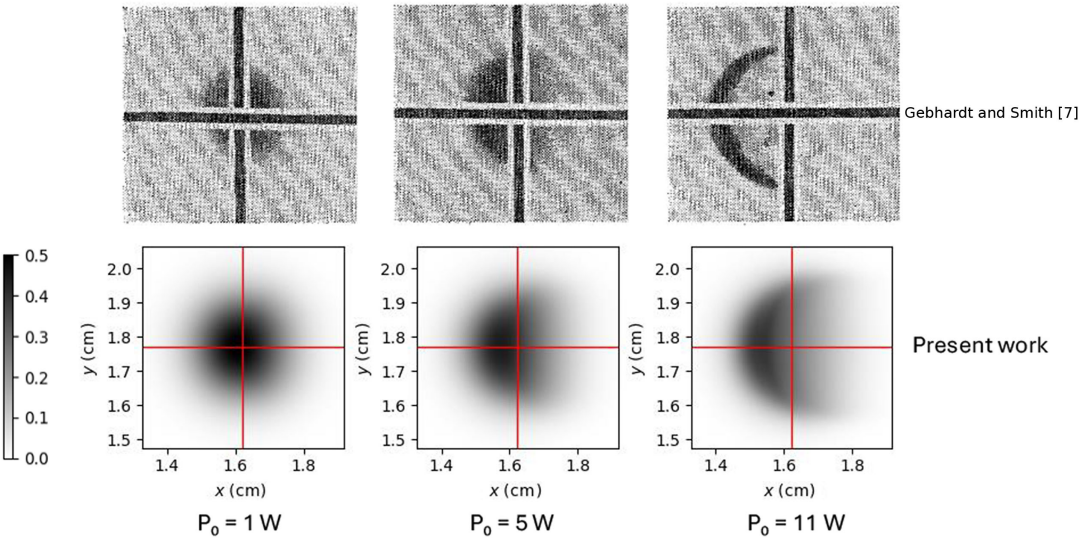

Fig. 4 Comparison of experimental [7] and computational laser intensity profiles at $z = L_z$. In the present work, normalized beam intensity (I/I_0) is shown. Cross hairs indicate beam center at $z = 0$.

simulation with those from the reference experiment in Fig. 4. The intensity profiles showed acceptable agreement. At this time, the laser beam reached the middle of the domain and exhibited an almost steady-state behavior. Because the experiment did not specify the exact time of the intensity profile, we assumed it represented a steady-state profile as well. The temperature profile in the $y = L_y/2$ plane for the 11 W laser case at 1.8 s is shown in Fig. 5. A quantitative comparison between the numerical and experimental results was conducted as shown in Fig. 6. Here, Δx represents the horizontal distance between the location of peak intensity at the exit plane and the beam center at the inlet plane, whereas I_p denotes the peak intensity of the laser beam at the exit plane. The cluster of data points by Gebhardt and Smith corresponds to N_D values obtained from combinations of P_0, $\beta_a L_z$, and u values. Given the approximations in the governing equations and simulation parameters, the numerical results show satisfactory agreement with the experimental data.

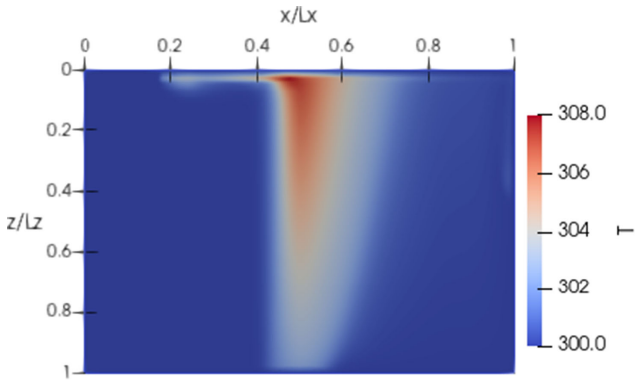

Fig. 5 Temperature (in Kelvin) profile in the $y = L_y/2$ plane at $t = 1.8$ s, for $P_0 = 11$ W case.

V. Conclusions

To investigate laser–fluid interaction within closed domains, a 3-D solver, `icoLfiFoam`, was developed for uniform grids. Within the OpenFOAM toolbox, the built-in `icoFoam` fluid solver was essentially augmented with capabilities for solving the coupled laser and fluid dynamics. The solver was validated for two test cases: 1) laser beam diffraction while propagating in a vacuum, and 2) thermal distortion of a moving laser beam propagating through a fluid cell.

The obtained results are consistent with physical principles, and align closely with experimental findings available in the literature. A parametric study of laser–fluid interaction in closed domains is currently being conducted using the present solver. In the future, this solver will be extended to explore flow-conditioning strategies aimed at controlling beam distortion. This will require extending the paraxial equation solver to handle geometries involving nonuniform structured or unstructured grids.

Acknowledgments

We acknowledge the use of the Aerospace Computational Engine facility at the Department of Aerospace Engineering, Indian

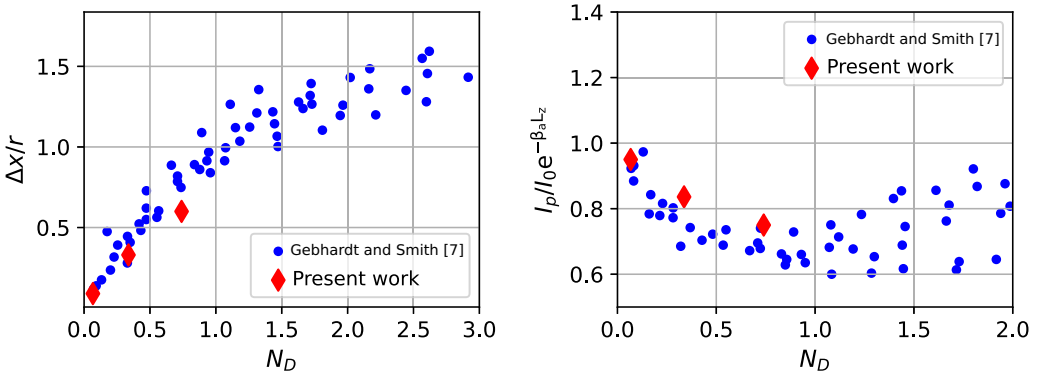

Fig. 6 Experimental and numerical plot of the normalized beam deflection ($\Delta x/r$) and the normalized beam peak intensity ($I_p/I_0 e^{-\beta_a L_z}$) in the $z = L_z$ plane as functions of N_D.

Downloaded by Indian Institute of Technology, Bombay on November 26, 2025 | http://arc.aiaa.org | DOI: 10.2514/1.T7232

Institute of Technology Bombay. Additionally, we used the artificial intelligence tool GPT-4o for language review and rephrasing to enhance clarity.

References

[1] Phipps, C. R., "Overview of Laser Applications: the State of the Art and the Future Trend," *Third International Symposium on Laser Precision Microfabrication*, Vol. 4830, International Soc. for Optics and Photonics, SPIE, Bellingham, WA, 2003, pp. 1–10. https://doi.org/10.1117/12.486517

[2] Mallik, A., "Lasers in Defense," *Photonic Systems and Applications in Defense and Manufacturing*, Vol. 3898, International Soc. for Optics and Photonics, SPIE, Bellingham, WA, 1999, pp. 104–114. https://doi.org/10.1117/12.368516

[3] McDonald, H., and Chen, K. F., "Laser Thermal Beamed Energy Propulsion Feasibility Study," *AIAA SCITECH 2024 Forum*, AIAA Paper 2024-1810, 2024. https://doi.org/10.2514/6.2024-1810

[4] Jin, K., and Zhou, W., "Wireless Laser Power Transmission: A Review of Recent Progress," *IEEE Transactions on Power Electronics*, Vol. 34, No. 4, 2019, pp. 3842–3859. https://doi.org/10.1109/TPEL.2018.2853156

[5] Gebhardt, F. G., "Twenty-Five Years of Thermal Blooming: An Overview," *Propagation of High-Energy Laser Beams Through the Earth's Atmosphere*, Vol. 1221, International Soc. for Optics and Photonics, SPIE, Bellingham, WA, 1990, pp. 2–25. https://doi.org/10.1117/12.18326

[6] Wang, L., and Lin, W., "The Effect of Wind Directions on the Thermal Blooming of a Laser Beam Propagating in the Air," *Journal of Russian Laser Research*, Vol. 37, No. 4, 2016, pp. 407–410. https://doi.org/10.1007/s10946-016-9589-1

[7] Gebhardt, F., and Smith, D., "Self-Induced Thermal Distortion in the Near Field for a Laser Beam in a Moving Medium," *IEEE Journal of Quantum Electronics*, Vol. 7, No. 2, 1971, pp. 63–73. https://doi.org/10.1109/JQE.1971.1076598

[8] Ahn, K., Lee, S.-H., Park, I.-K., and Yang, H.-S., "Numerical Simulation of High-Energy Laser Propagation Through the Atmosphere and Phase Correction Based on Adaptive Optics," *Journal of the Korean Physical Society*, Vol. 79, No. 10, 2021, pp. 918–929. https://doi.org/10.1007/s40042-021-00293-x

[9] Fleck, J. A., Morris, J., and Feit, M., "Time-Dependent Propagation of High Energy Laser Beams Through the Atmosphere," *Applied Physics*, Vol. 10, No. 2, 1976, pp. 129–160. https://doi.org/10.1007/BF00896333

[10] Holmes, R. B., "Adaptive Optics for Directed Energy: Fundamentals and Methodology," *AIAA Journal*, Vol. 60, No. 10, 2022, pp. 5633–5644. https://doi.org/10.2514/1.J061766

[11] Akers, B. F., and Reeger, J. A., "Numerical Simulation of Thermal Blooming with Laser-Induced Convection," *Journal of Electromagnetic Waves and Applications*, Vol. 33, No. 1, 2019, pp. 96–106. https://doi.org/10.1080/09205071.2018.1528183

[12] Stephens, T., Johnson, D. C., and Languirand, M. T., "Beam Path Conditioning for High-Power Laser Systems," *Lincoln Laboratory Journal*, Vol. 3, No. 2, 1990, pp. 225–244.

[13] Johnson, D. C., and Holderbaum, G. S., "Beam Path Conditioning for High Energy Laser Beam Directors," *Propagation Engineering: Third in a Series*, Vol. 1312, International Soc. for Optics and Photonics (SPIE), Bellingham, WA, 1990, pp. 422–442. https://doi.org/10.1117/12.21900

[14] Rennie, R. M., Jumper, E. J., and Marineau, E. C., "Investigation of the Importance of Convective Heat Transfer on Laser-Induced Heating," *Journal of Thermophysics and Heat Transfer*, Vol. 24, No. 3, 2010, pp. 573–580. https://doi.org/10.2514/1.47657

[15] Rivière, D., Selva, B., Chraibi, H., Delabre, U., and Delville, J.-P., "Convection Flows Driven by Laser Heating of a Liquid Layer," *Physical Review E*, Vol. 93, No. 2, 2016, Paper 023112. https://doi.org/10.1103/PhysRevE.93.023112

[16] Wang, M., Mani, A., and Gordeyev, S., "Physics and Computation of Aero-Optics," *Annual Review of Fluid Mechanics*, Vol. 44, No. 1, 2012, pp. 299–321. https://doi.org/10.1146/annurev-fluid-120710-101152

[17] Vukasinovic, B., Glezer, A., Gordeyev, S., Jumper, E., and Kibens, V., "Fluidic Control of a Turret Wake: Aerodynamic and Aero-Optical Effects," *AIAA Journal*, Vol. 48, No. 8, 2010, pp. 1686–1699. https://doi.org/10.2514/1.J050085

[18] White, M., and Visbal, M., "Aero-Optics of Compressible Boundary Layers in the Transonic Regime," *43rd AIAA Plasmadynamics and Lasers Conference*, AIAA Paper 2012-2984, 2012. https://doi.org/10.2514/6.2012-2984

[19] Tritton, D. J., *Physical Fluid Dynamics*, Springer, Dordrecht, 2012, pp. 127–130. https://doi.org/10.1007/978-94-009-9992-3

[20] Strohbehn, J. W., *Laser Beam Propagation in the Atmosphere, Topics in Applied Physics*, Vol. 25, Springer, Berlin, 1978, pp. 230–233. https://doi.org/10.1007/3-540-08812-1

[21] "OpenFOAM/openfoam-10," 2024, https://github.com/OpenFOAM/OpenFOAM-10 [retrieved 20 June 2024].

[22] Weller, H. G., Tabor, G., Jasak, H., and Fureby, C., "A Tensorial Approach to Computational Continuum Mechanics Using Object-Oriented Techniques," *Computers in Physics*, Vol. 12, No. 6, 1998, pp. 620–631. https://doi.org/10.1063/1.168744

[23] Mross, C., "Numerical Solutions to Paraxial Wave Equations," Master Thesis, Delaware State Univ., Dover, Delaware, 2018.

[24] Weideman, J. A. C., and Herbst, B. M., "Split-Step Methods for the Solution of the Nonlinear Schrödinger Equation," *SIAM Journal on Numerical Analysis*, Vol. 23, No. 3, 1986, pp. 485–507. https://doi.org/10.1137/0723033

[25] Frigo, M., and Johnson, S. G., "The Design and Implementation of FFTW3," *Proceedings of the IEEE*, Vol. 93, No. 2, 2005, pp. 216–231. https://doi.org/10.1109/JPROC.2004.840301

[26] Svelto, O., and Hanna, D. C., *Principles of Lasers*, Vol. 1, Springer, New York, 2010, pp. 153–155. https://doi.org/10.1007/978-1-4419-1302-9

J. I. Frankel
Associate Editor

Downloaded by Indian Institute of Technology, Bombay on November 26, 2025 | http://arc.aiaa.org | DOI: 10.2514/1.T7232